Electrochemical and Solid-State Letters, **13** (8) A115-A117 (2010)
1099-0062/2010/13(8)/A115/3/$28.00 © The Electrochemical Society

Mapping of Heterogeneous Chemical States of Lithium in a $LiNiO_2$-Based Active Material by Electron Energy-Loss Spectroscopy

Shunsuke Muto,[a,z] Kazuyoshi Tatsumi,[a] Tsuyoshi Sasaki,[b,*] Hiroki Kondo,[b] Tetsu Ohsuna,[b] Kayo Horibuchi,[b] and Yoji Takeuchi[b]

[a]*Department of Materials, Physics and Energy Engineering, Graduate School of Nagoya University, Nagoya 464-8603, Japan*
[b]*Toyota Central Research and Development Laboratories Incorporated, Nagakute 480-1192, Japan*

It is difficult to analyze the local concentrations and chemical states of lithium in lithium-ion secondary battery electrodes by microanalysis techniques based on transmission electron microscopy because the core excitation spectra of transition metals invariably overlap with the absorption/emission spectra of Li–K. We propose a promising analysis method that enables the spatial distribution of lithium with different chemical states from the original phase in a $LiNiO_2$-based positive electrode to be visualized. It employs a suite of spectrum imaging techniques including scanning transmission electron microscopy, electron energy-loss spectroscopy, and multivariate curve resolution. This method is successfully applied to a cross-sectioned positive electrode.
 [DOI: 10.1149/1.3439641]

Manuscript submitted March 15, 2010; revised manuscript received April 14, 2010. Published June 1, 2010.

Among lithium transition-metal oxides, $LiNiO_2$-based materials are considered to be the promising material for producing positive electrodes in lithium-ion secondary batteries for high power applications. In the research and development of lithium-ion secondary batteries, it is crucial to investigate the chemical states of lithium in localized regions because battery performance is highly dependent on reversible extractions and insertions of Li ions at the electrode materials' surface during charge–discharge cycles. However, no techniques for achieving this have been established. NMR has been successfully used to observe the diffusion of ^{7}Li nuclei,[1] but it can only provide data averaged over the entire electrode. High resolution transmission electron microscopy (TEM) has opened up the possibility of directly observing lithium,[2,3] but like electron diffraction techniques, it is limited to highly crystalline and orientated materials.

A promising alternative is electron energy-loss spectroscopy (EELS). It probes the local chemical bonding environments of specific elements and is particularly effective for light elements. Recent nanobeam technologies enable information to be obtained from atomic-scale regions by focusing an electron beam down to a very small area on a sample. By scanning the electron beam over the entire region of interest, it is possible to visualize the spatial distributions of a specific element and electronic states; this technique is known as EELS spectrum imaging (SI).[4] However, because in promising materials for positive electrodes (e.g., $LiMn_2O_4$, $LiMO_2$ (M = Ni, Co, Mn), and $LiFePO_4$) the transition-metal (TM: Mn, Fe, Co, Ni) $M_{2,3}$ edges (TM $3p \rightarrow 4d^*$) and the Li K edge (Li $1s \rightarrow 2p^*$) have very similar energy losses, it is not possible to extract information on lithium from spectra by merely selecting the lithium absorption edge with an energy slit. Kikkawa et al. determined the distributions of lithium in $Li_{1.2}Mn_{0.4}Fe_{0.4}O_2$ particles by taking the second derivative of each spectrum to separate the primary sharp peak of the Li–K energy-loss near-edge structure (ELNES) from the overlapping $M_{2,3}$ edges of the transition metals.[5] However, this method cannot be used to investigate the chemical states of lithium and other elements because it does not permit entire spectral fine structures to be extracted.

We have recently developed a method for separating the overlapping mixed spectra in SI data into individual component spectra, enabling the concentration distribution of each component to be determined by applying multivariate curve resolution (MCR).[6,7] This technique resolves mixed spectra into a linear combination of a prespecified number of components by least-squares fitting. It has been successfully applied to scanning transmission electron microscopy (STEM) EELS SI data obtained from a positive electrode made from $LiNi_{0.8}Co_{0.15}Al_{0.05}O_2$ (NCA), a positive electrode material.[7] In the present study, we perform direct analysis and spatial mapping of Li K ELNES in a low loss region by applying MCR to SI data from the low loss spectral region of the same type of sample. While principal component analysis (PCA) has been applied to SI data, PCA solutions are not physically meaningful from the viewpoint of spectral fine structures.[6]

Experimental

Positive electrodes were fabricated from NCA, conductive carbon, and poly(vinylidene fluoride) binder.[8] The positive electrodes were assembled into cylindrical cells with graphite negative electrodes and 1 M $LiPF_6$–ethylene carbonate/diethyl carbonate (DEC) electrolyte solution. After a few initial charge/discharge cycles, the cell was discharged to 3.0 V and then disassembled. The positive electrode was collected and washed in DEC to remove any residual electrolyte solution. A TEM thin film was prepared by focused ion beam thinning to produce a thin film (~100 nm thick) over an area as large as ~10 μm, which is equivalent to the area of a secondary particle.

SI data were acquired at room temperature using a JEOL JEM2100 S/TEM equipped with a Gatan Enfina 1000 spectrometer using a probe size of 6 nm, an acquisition time of 0.8 s, and a scan step of 30 nm. The energy dispersion was set to 0.1 eV/channel and the energy-loss range was set from −10 to 120 eV including the zero loss peak (ZLP). The collected spectra were aligned so that the ZLPs were located at the zero energy position. They were then deconvolved by the Fourier-log method to remove the ZLPs and multiple loss components.[9] The Li K, Co, and Ni $M_{2,3}$ ELNES spectra start at around 58–65 eV so that they lie on the high energy tail of the volume plasmon peak. The spectra were then carefully isolated by subtracting the pre-edge background using a power law and selecting an appropriate pre-edge region to extract the core-loss spectra of 56–80 eV. We also subtracted the pre-edge background using a polynomial function and a first-order log-polynomial function,[9] which may sometimes yield a better fit; however, there was no significant improvement in the core-loss spectra extraction when we did this.

Results and Discussion

Figure 1a shows an annular dark-field (ADF) STEM image of a secondary particle of the active material. The particle is an agglomeration of small primary particles with random orientations. Grains that satisfy the conditions for strong Bragg reflection have bright contrasts. SI was conducted in the region inside the frame in Fig. 1a

* Electrochemical Society Active Member.
z E-mail: s-mutoh@nucl.nagoya-u.ac.jp

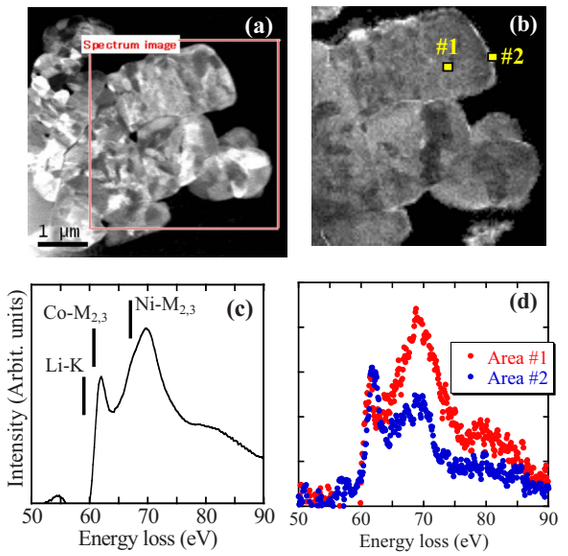

Figure 1. (Color online) (a) ADF image of active material particles in NCA positive electrode. (b) Spectral image of the framed area in (a) for the Li–K ELNES region with the pre-edge background subtracted and the image intensities averaged over the core-loss spectra. (d) Extracted spectra from points 1 and 2 indicated in (b). The thresholds for Li–K, Co–, and Ni–$M_{2,3}$ edges are indicated in the averaged spectrum (c).

and the average intensities along the energy axis are shown in Fig. 1b. Areas with a strong diffraction contrast in Fig. 1a appear dark in Fig. 1b. This is because incoming electrons are strongly scattered to the ADF detector from the bright regions in Fig. 1a so that there are less forward scattered electrons, which makes the total EELS intensity weaker than that from other regions.

We first attempted to obtain EELS spectra from the two positions marked in Fig. 1b, as shown in Fig. 1d, because the peripheries of the particle surfaces at these points exhibit bright contrast. The expected onsets of Li–K, Co–$M_{2,3}$, and Ni–$M_{2,3}$ ELNES are indicated in Fig. 1c. Because the latter two exhibit delayed maxima, the sharp peak at ~60 eV is expected to belong to Li–K ELNES. Other features are all contained in the broad peak appearing at 63–75 eV. In contrast to the EELS spectrum from area 1, the spectrum from area 2 has a sharp peak at ~60 eV that is significantly higher in intensity than the broad peak on the high energy side, implying that different compositions and chemical states are present in these areas. The MCR technique was then applied to the data sets to resolve the spectral components by increasing the number of components until the spatial distribution of the residual component exhibits only statistical noise having no significant texture that correlates with the microstructure.

Figure 2a-d shows the spatial distributions of the resolved components, assuming that there are four components. The spectral profiles of the pure components are shown in Fig. 3. Because MCR assumes that the spectral profile at each position is a linear combination of the spectra of the pure components, it can extract the

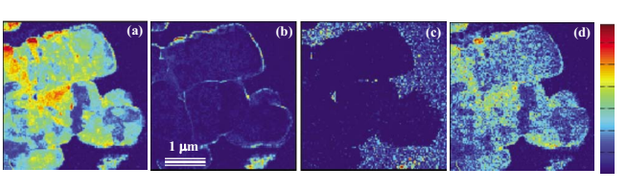

Figure 2. (Color online) Projected spatial distributions of components 1–4 resolved by applying MCR to the spectral image shown in Fig. 1b corresponding to the spectra shown in Fig. 3.

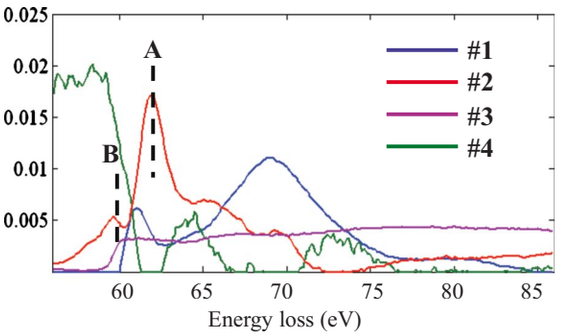

Figure 3. (Color online) Resolved spectral components 1–4.

underlying components only when the weight (composition) of each component spectrum changes independently of spatial position.[10] Bearing this in mind and by inspecting the resolved components in Fig. 3 and their spatial distributions in Fig. 2a-d, we can assign the four components. Component 1 can be assigned to the same component in Fig. 1c (i.e., the same spectrum from area 1 in Fig. 1b); this component is always isolated as the main component. Specifically, it is an inseparable combination of the spectra of Li–K, Co–$M_{2,3}$, and Ni–$M_{2,3}$ of the initial NCA phase with a uniform composition. Component 2 is considered to be a Li-related phase in a different chemical state. Component 3 seems to be the remnants of the pre-edge background, and the second and third plasmon peaks principally derived from the carbon and binder regions, respectively, judging from their spatial distribution and spectral fraction (~5%). Finally, component 4, which accounts for a significant fraction of the spectra, can be interpreted as being the variation in the postedge background due to variation in the specimen thickness. We confirmed the uniqueness of the spectral decomposition by two different methods. First, the MCR procedure was applied to another secondary particle, and identical spectral profiles for components 1 and 2 with similar spatial distributions were obtained. Second, we performed a dynamic Monte Carlo search[11] for all the feasible solutions under the present constraints imposed on the solutions to the present data sets. The procedure successfully defined the boundaries of allowable pure component profiles and indicated that components 1 and 2 were nearly unique solutions within the present statistical accuracy, irrespective of the pre-edge background model used. The intensity of component 4 varied appreciably from particle to particle and when different prebackground models were used, suggesting that it is not a physically significant component.

The main sharp peak (peak A in Fig. 3) of component 2 is shifted to the high energy side relative to that of component 1; this peak and prepeak B are not clearly visible by the point-to-point analysis (see Fig. 1c), but they become visible after applying MCR and extracting the statistical tendencies from many sampling points. This is partly because multiple states overlap within the sample thickness in the projected direction and partly because of the low signal-to-noise ratio obtained from a single spot. However, we previously reported[7] that fluorine was found on the primary particle surfaces, presumably because chemical reactions during the charge–discharge cycle occur at surface regions that are in contact with the $LiPF_6$ electrolyte. The thickness of the fluorine-containing surface regions corresponds well to that of component 2. A small amount (i.e., a few atomic percent) of phosphorus was also found in the same regions as fluorine (not shown). Possible candidates for component 2 are thus lithium fluorides that are produced by decomposition or a reaction of the electrolyte, as recently reported.[12]

To clarify the origin of component 2, we compared it with the theoretical Li–K ELNES spectra of several conceivable candidates among the Li compounds. Because experimental Li–K ELNES spectra from Li–P–F derivatives are not always available, we calculated the theoretical spectra for $LiNiO_2$, LiF, $LiPF_6$, and other pos-

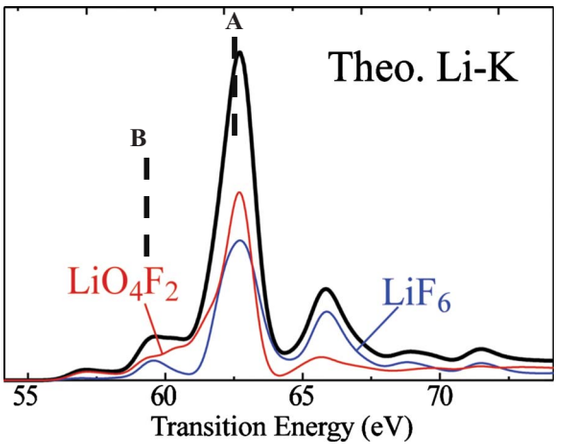

Figure 4. (Color online) Simulated Li–K ELNES spectrum (black solid line) for $Li_xPO_yF_z$ by the PAW method within the generalized gradient approximation (WIEN2k). The spectrum consists of two distinct peaks from the two local atomic configurations, as shown by red and blue lines.

sible compounds[12] using the projected augmented wave (PAW) method within the generalized gradient approximation WIEN2k[13,14] to compare the relative peak intensities and positions. The energy-loss axis was calibrated using the experimental and theoretical spectra of Li_2O and $LiNiO_2$. We did not take the Co– and Ni–$M_{2,3}$ ELNES into consideration in the calculation because the product Li–P–F derivatives contain little Co and Ni. Even if component 2 does contain Co– and Ni–$M_{2,3}$ spectra, the characteristic peaks A and B should be derived solely from the Li–K ELNES because of the delayed maxima of Co– and Ni–$M_{2,3}$ ELNES. Of the theoretically predicted spectra, the positions of the two characteristic peaks best agree with that of $Li_xPO_yF_z$-type materials group (i.e., based on the $LiPF_6$ structure; x, y, z are adjustable parameters to ensure electrical neutrality), which was suggested as an electrolyte derivative[12] (see Fig. 4). In Li–K ELNES for which transitions from shallow core states are studied, theoretical predictions based on density functional theory generally do not reproduce the experimental spectra well, particularly the peak separation and relative peak intensities.[15] A recent theoretical scheme that involves solving the electron/core–hole Bethe–Salpeter equation (BSE) partly improves the situation.[15] However, the BSE scheme cannot be currently applied to complex structures such as the present case due to its very high computational cost. The discrepancy between the theoretical spectra in Fig. 4 and the experimental one is not considered to be due to disregarding the transition metals, but rather it is ascribed to the limitations of the discrete Fourier transform scheme. Other conceivable chemical states of lithium such as Li occupying the Ni site, Li replacing Ni in the rocksalt-type phase, and the LiF phase can be readily excluded as possible candidates based on the significant discrepancies in the spectral profile. The experimentally observed chemical shifts of the main peak A and the prepeak B (see Fig. 3) can be derived from the local atomic configurations (Li and its six nearest-neighbor atoms) of LiO_4F_2 and LiF_6 clusters, as shown in Fig. 4. This result is consistent with a recent X-ray photoelectron spectroscopy surface analysis.[12] The present method revealed that the product phase is distributed not only over the surface of the secondary particles but also along the grain boundaries between the primary particles of the active material. Because the unstable residual $LiPF_6$ may decompose and be partially oxidized, component 2 in Fig. 3 may be due to a mixture of different combinations of y and z that form LiO_iF_{6-i}-type local configurations rather than a single phase. The present method has the potential to be a key technique for the degradation analysis of lithium batteries after many cycling tests and storage at elevated temperatures because it enables us to directly analyze lithium and to visualize the spatial distributions and relative concentrations of the chemical states in the nanometer scale.[16] In degraded samples that had been subjected to many cycling tests, lithium in the NiO-like degraded phase is separate from the SI data set, and Co– and Ni–$M_{2,3}$ ELNES are also isolated because of local composition changes resulting from electrode degradation; these results will be published elsewhere.

Acknowledgment

This work was supported in part by a grant-in-aid for Scientific Research (KAKENHI) in priority area (no. 474) "Atomic Scale Modification" and "Kiban-Kenkyu B" (no. 21360321) from MEXT, Japan.

Nagoya University assisted in meeting the publication costs of this article.

References

1. C. P. Grey and N. Dupr, *Chem. Rev. (Washington, D.C.)*, **104**, 4493 (2004).
2. Y. Shao-Horn, L. Croguennec, C. Delmas, E. C. Nelson, and M. A. O'Keefe, *Nature Mater.*, **2**, 464 (2003).
3. S.-Y. Chung, S.-Y. Choi, T. Yamamoto, and Y. Ikuhara, *Phys. Rev. Lett.*, **100**, 125502 (2008).
4. C. Jeanguillaume and C. Colliex, *Ultramicroscopy*, **28**, 252 (1989).
5. J. Kikkawa, T. Akita, M. Tabuchi, M. Shikano, K. Tatsumi, and M. Kohyama, *Electrochem. Solid-State Lett.*, **11**, A183 (2008).
6. S. Muto, T. Yoshida, and K. Tatsumi, *Mater. Trans.*, **50**, 964 (2009).
7. S. Muto, Y. Sasano, K. Tatsumi, T. Sasaki, K. Horibuchi, Y. Takeuchi, and Y. Ukyo, *J. Electrochem. Soc.*, **156**, A371 (2009).
8. Y. Itou and Y. Ukyo, *J. Power Sources*, **146**, 39 (2005).
9. R. F. Egerton, *Electron Energy-Loss Spectroscopy*, p. 246, Plenum, New York (1996).
10. J.-H. Wang, P. K. Hopke, T. M. Hancewicz, and S. L. Zhang, *Anal. Chim. Acta*, **476**, 93 (2003).
11. M. C. Leger and P. D. Wentell, *Chemom. Intell. Lab. Syst.*, **62**, 171 (2002).
12. M. Xu, A. Xiao, W. Li, and B. L. Lucht, *J. Electrochem. Soc.*, **157**, A115 (2010).
13. P. Blaha, K. Schwalz, G. K. H. Madsen, D. Kvasnicka, and J. Luitz, in *WIEN2k, An Augmented Plane Wave + Local Orbitals Program for Calculating Crystal Properties*, K. Schwarz, Editor, Technische Universität Wien, Austria (2001).
14. K. Tatsumi, Y. Sasano, S. Muto, T. Yoshida, T. Sasaki, K. Horibuchi, Y. Takeuchi, and Y. Ukyo, *Phys. Rev. B*, **78**, 045108 (2008).
15. W. Olovsson, I. Tanaka, T. Mizoguchi, P. Puschnig, and C. Ambrosch-Draxl, *Phys. Rev. B*, **79**, 041102 (2009).
16. S. Muto, K. Tatsumi, T. Sasaki, K. Horibuchi, T. Ohsuna, H. Kondo, and Y. Takeuchi, Abstract 547, The Electrochemical Society Meeting Abstracts, Vol. 2009-02, Vienna, Austria, Oct 4–9, 2009.